ARTHRITIS & RHEUMATISM
Vol. 65, No. 7, July 2013, pp 1736–1746
DOI 10.1002/art.37981

Evidence That CXCL16 Is a Potent Mediator of Angiogenesis and Is Involved in Endothelial Progenitor Cell Chemotaxis

Studies in Mice With K/BxN Serum–Induced Arthritis

Takeo Isozaki,[1] Ali S. Arbab,[2] Christian S. Haas,[1] M. Asif Amin,[1] Monica D. Arendt,[1] Alisa E. Koch,[3] and Jeffrey H. Ruth[1]

Objective. **To examine the possibility that CXCL16 recruits endothelial cells (ECs) to developing neovasculature in rheumatoid arthritis (RA) synovium.**

Methods. **We utilized the RA synovial tissue SCID mouse chimera system to examine human microvascular EC (HMVEC) and human endothelial progenitor cell (EPC) recruitment into engrafted human synovium that was injected intragraft with CXCL16-immunodepleted RA synovial fluid (SF). CXCR6-deficient and wild-type (WT) C57BL/6 mice were primed to develop K/BxN serum–induced arthritis and evaluated for angiogenesis. HMVECs and EPCs from human cord blood were also examined for CXCR6 expression, by immunofluorescence and assessment of CXCL16 signaling activity.**

Results. **CXCR6 was prominently expressed on human EPCs and HMVECs, and its expression on HMVECs could be up-regulated by interleukin-1β. SCID mice injected with CXCL16-depleted RA SF exhibited a significant reduction in EPC recruitment. In experiments using the K/BxN serum–induced inflammatory arthritis model, CXCR6$^{-/-}$ mice showed profound reductions in hemoglobin levels, which correlated with reductions in monocyte and T cell recruitment to arthritic joint tissue compared to that observed in WT mice. Additionally, HMVECs and EPCs responded to CXCL16 stimulation, but exhibited unique signal transduction pathways and homing properties.**

Conclusion. **These results indicate that CXCL16 and its receptor CXCR6 may be a central ligand/receptor pair that is closely associated with EPC recruitment and blood vessel formation in the RA joint.**

Rheumatoid arthritis (RA) is a debilitating inflammatory joint disorder affecting ~2% of the population worldwide (1). Autoimmune-mediated inflammation has long been known to be the primary mechanistic component of the cartilage and bone destruction observed in RA joints (2). Growth of new blood vessels (i.e., neovascularization) in the joint lining (synovium) is characteristic of this inflammatory response and is observed early in RA pathogenesis (3).

Synovial neovascularization plays a pivotal role in the progression of RA, by creating a direct conduit by which circulating leukocytes that exacerbate inflammation can enter the joint. Neovascularization occurs by one of two mechanisms: angiogenesis (the replication and reorganization of preexisting microvascular endothelial cells [ECs]) (4) or vasculogenesis (the recruitment of endothelial progenitor cells [EPCs] that

Supported by a pilot project grant from the University of Michigan Rheumatic Diseases Research Core Center (which is funded by NIH grant P30-AR-048310) and by NIH grants AI-40987, HL-58694, AR-48267, and R01-CA-122031. Dr. Haas' work was supported by an American Heart Association Postdoctoral Fellowship (AHA0423758Z). Dr. Koch's work was supported by the Office of Research and Development, Medical Research Service, Department of Veterans Affairs and by the Frederick G. L. Huetwell and William D. Robinson, MD, Professorship in Rheumatology at the University of Michigan.

[1]Takeo Isozaki, MD, PhD, Christian S. Haas, MD, M. Asif Amin, MD, Monica D. Arendt, BS, Jeffrey H. Ruth, PhD: University of Michigan Medical School, Ann Arbor; [2]Ali S. Arbab, MD, PhD: Henry Ford Hospital and Medical Centers, Detroit, Michigan; [3]Alisa E. Koch, MD: University of Michigan Medical School and VA Healthcare System, Ann Arbor, Michigan (current address: Lilly USA, Indianapolis, Indiana).

Dr. Koch owns stock or stock options in Lilly USA.

Address correspondence to Jeffrey H. Ruth, PhD, University of Michigan Medical School, Department of Medicine, Division of Rheumatology, 109 Zina Pitcher Drive, 4023 BSRB, Box 2200, Ann Arbor, MI 48109-2200. E-mail: jhruth@med.umich.edu.

Submitted for publication November 16, 2012; accepted in revised form April 11, 2013.

subsequently incorporate into the existing tissue and differentiate into mature functional ECs) (5).

Chemokines are small soluble molecules that recruit destructive proinflammatory immune cells to RA synovium. Some CXC chemokines exhibit angiogenic activity (6–9). Although studies to characterize the actions of chemokines have identified many in vitro functions, there is still a need for information regarding the specific role of chemokines in animal models of RA. Interestingly, a recent study showed that a high percentage of primary bone marrow–derived murine mesenchymal stem cells (mean ± SEM 96 ± 2%) expressed CXCR6, the only known receptor for CXCL16, on their cell surface; of note, CXCR6 was expressed on a high proportion of human bone marrow–derived mesenchymal stem cells as well (95 ± 1%) (10). Considering the known function of this receptor in relation to recruitment and homing of immune cells (11), it is reasonable to hypothesize that CXCR6 may also be involved in the recruitment and homing of mesenchymal stem cells to inflamed tissue, likely for the purpose of tissue regeneration and/or vasculogenesis (10).

There is growing evidence suggesting that EPCs contribute to the homeostasis of the physiologic vascular network (12) and, additionally, contribute to vascular remodeling of RA synovium by recruiting bone marrow–derived circulating EPCs (13). We have previously demonstrated very highly elevated concentrations of soluble CXCL16 compared to other chemokines in RA synovial fluid (SF) (11). Our present data show that CXCL16 has a distinct role as an important factor in EC angiogenesis and EPC recruitment to human synovium in vivo. We found that both human microvascular ECs (HMVECs) and EPCs express CXCR6 and that HMVECs up-regulate CXCR6 in response to proinflammatory stimuli. Thus, we believe selective regulation of EC-mediated migration may be a viable therapeutic strategy for limiting vasculogenesis in RA synovium.

MATERIALS AND METHODS

Rodents. Animal care at the Unit for Laboratory Animal Medicine at the University of Michigan is supervised by a veterinarian and operated in accordance with federal regulations. SCID mice were obtained from the National Cancer Institute. Breeder pairs of CXCR6-knockout C57BL/6 mice (a kind gift from Dr. Daniel R. Littman, New York University, New York, NY) and age- and weight-matched wild-type (WT) C57BL/6 mice were bred in-house according to the guidelines of the University Committee on the Use and Care of Animals. All experiments were performed on female mice and were initiated when the animals were 4–6 weeks old. The mice were provided food and water ad libitum throughout the entire study and were housed in sterile rodent microisolator caging with filtered cage tops in a specific pathogen–free environment. All efforts were made to reduce stress or discomfort to the animals.

Isolation of CD34+ EPCs from cord blood. Human EPCs were isolated from cord blood from granulocyte colony-stimulating factor–mobilized leukapheresis samples on the basis of CD133 expression, using an antibody-coupled magnetic bead cell isolation system (Stem Cell Technologies). Human umbilical cord blood was collected by the method of Moore et al (14), as previously described (13). To confirm purity of the EPCs, isolated cell populations were analyzed by flow cytometry as previously described (15,16). EPCs with appropriate cell markers (CD34+, CD133+, CD14−) were used in chimeras and related in vitro studies.

Fluorescence microscopy of ECs. HMVECs (passage 9 or lower) were plated, on 8-well Lab-Tek chamber slides at 20,000/well, in 0.1% bovine serum albumin endothelial basal medium (EBM) without antibiotics. Some HMVECs were stimulated with interleukin-1β (IL-1β) for 24 hours. The next day, cells were washed with phosphate buffered saline (PBS) and fixed with 4% formalin for 30 minutes at room temperature, washed again with PBS, and fixed with cold acetone for 20 minutes. EPCs were also plated at 20,000/well in 8-well Lab-Tek chamber slides in Stem-span and fixed similarly. For staining, HMVECs and EPCs were blocked with 20% fetal bovine serum (FBS) and 5% donkey serum for 1 hour at 37°C. Mouse anti-human CXCR6 antibody (R&D Systems) or mouse anti-human von Willebrand factor (vWF) antibody (Dako) was used as primary antibody. Fluorescence-conjugated secondary antibody was purchased from Molecular Probes, and cell nuclei were stained with DAPI (Molecular Probes).

Immunofluorescence analysis for leukocytes. Immunofluorescence histologic analysis was performed as previously described (11). Briefly, rat anti-mouse CD3 or CD14 antibodies (final concentration 10 μg/ml; both from BD Biosciences) were added as primary antibodies and incubated for 1 hour at 37°C. Rat IgG was used as a negative control. After washing twice with PBS, Alexa Fluor 488–labeled goat anti-rat antibody was added and incubated for 1 hour at 37°C. After washing with PBS, nuclei were counterstained with DAPI and coverslipped. Serial sections were examined with a BX51 Fluorescence Microscope System using DP Manager imaging software (Olympus). Photographs were merged, and CD3+ or CD14+ macrophages were identified by fluorescence microscopy.

HMVEC chemotaxis assay. HMVECs (BioWhittaker) were maintained in growth factor complete EBM supplemented with 10% FBS. Cells (from passage 7–10) did not display discernible phenotypic changes when observed before each assay. Cells were maintained at 37°C in a 5% CO_2 atmosphere. HMVEC migration in vitro was tested using a modified 48-well Boyden chemotaxis chamber (Neuro Probe) as previously described (17), and the data were expressed as the number of cells migrating per well.

In vitro capillary morphogenesis assay. HMVECs were suspended in EBM with 0.1% FBS and seeded in Lab-Tek chamber slides on growth factor–reduced Matrigel (Becton Dickinson) at a density of 1.6×10^4 cells per chamber. Immediately after plating, cells were treated with recombinant

human CXCL16 (100 ng/ml), 4-phorbol 12-myristate 13-acetate (PMA; 50 nmoles/liter) (as a positive control), or DMSO (included as a negative control since PMA is dissolved in DMSO). After 18 hours, capillary morphogenesis was examined by phase-contrast microscopy and node formation evaluated by an investigator who was blinded with regard to the experimental setup. Capillary formation was defined as the induction of a minimum of 3 separate capillary events by HMVECs in growth factor–reduced Matrigel, as previously described (17).

Western blotting and cell signaling in HMVECs and EPCs. Western blotting of ECs was performed as previously described (11,18). Briefly, HMVECs and EPCs were plated at 1×10^5 in 0.1% FBS/EBM (HMVECs) or Stem-span media (EPCs) and stimulated with CXCL16 (80 ng/ml). Blots were probed using rabbit antibodies to selected phosphorylated signaling molecules (anti–phospho-p38, anti–phospho-ERK-1/2, anti–phospho-JNK, and anti–phospho-Src; all from Cell Signaling Technology). The immunoblots were stripped and reprobed with rabbit antibody to the total form of each signaling molecule (containing phosphorylated and nonphosphorylated forms of the same molecule) to verify equal loading. In some experiments, HMVECs and EPCs were probed for CXCR6 expression with and without IL-1β stimulation. The immunoreactive protein bands were visualized by enhanced chemiluminescence (Amersham Biosciences). Densitometric analysis of the bands was performed using Un-Scan-It software, version 5.1 (Silk Scientific).

RA SF neutralization studies. For neutralization of CXCL16, diluted SF (1:300 with PBS) was preincubated with a neutralizing polyclonal goat anti-human CXCL16 antibody (catalog no. AF976; R&D Systems) at a concentration of 135 ng/100 μl diluted SF (from undiluted SF samples containing ~45 ng/ml CXCL16). Control (sham-depleted) SF samples were incubated in a similar manner but with a corresponding control nonspecific antibody (goat IgG), as recommended by the manufacturer (R&D Systems) and as previously described in experiments using RA SF (19).

K/BxN serum–induced arthritis model. To generate arthritic K/BxN mice, K/B mice were crossed with NOD/ShiLtJ mice as previously described (20). Naive mice (ages 5–7 weeks) were injected intraperitoneally with 150 μl of K/BxN mouse serum; the day of the first injection was considered to be day 0 of arthritis. Another injection of 150 μl of K/BxN mouse serum was administered on day 2. Robust arthritis with severe swelling of the joints typically developed on day 5. Articular index scores were determined and joint circumference measured starting on day 0 and at least every other day up to day 23 after induction of arthritis, as described previously for adjuvant-induced arthritis in the rat (21). Mouse ankles were harvested for histologic assessment or made into tissue homogenates.

Clinical assessment of K/BxN serum–induced arthritis. Clinical parameters in mice with arthritis were assessed from day 0 to day 23. The articular index consisted of a 0–4 scale, where 0 = no swelling or erythema, 1 = slight swelling and/or erythema, 2 = low-to-moderate edema, 3 = pronounced edema with limited use of the joint, and 4 = excessive edema with joint rigidity. Ankle circumference was determined as previously described (21). Briefly, 2 perpendicular diameters of the joint were measured with a caliper (Lange caliper; Cambridge Scientific), and ankle circumference was determined using the geometric formula $2\pi[\sqrt{(a^2 + b^2/2)}]$, where a is the laterolateral diameter and b is the anteroposterior diameter. In each ankle joint, the mean value of the 2 perpendicular diameters was calculated; these 4 values were then used to calculate the mean ankle circumference for the individual animal. Data are depicted as the increase in ankle circumference compared to the baseline (day 0) value. All measurements were performed by observers who were blinded with regard to the experimental conditions.

Determination of hemoglobin (Hgb) concentrations in ankle homogenates from mice with K/BxN–induced arthritis. For measurement of Hgb concentration (a reflection of the number of blood vessels in the tissue [17]), mouse joints were homogenized as previously described (22). Hgb levels were measured by adding 25 μl of homogenate mixed with 25 μl of 3,3′,5,5′-tetramethylbenzidine reagent to 96-well plates. Samples were incubated for 5 minutes at room temperature, and absorbance was read with a Microplate Manager enzyme-linked immunosorbent assay reader (BioTek Instruments) at 450 nm. Hgb concentrations were determined by comparison with a standard curve. Values were normalized by dividing the Hgb concentration by the amount of total protein in the homogenate.

HMVEC and EPC migration to engrafted tissue in the synovial tissue (ST) SCID mouse chimera. SCID mice were grafted as previously described (11). We utilized normal and RA ST SCID mouse chimeras to evaluate HMVEC and EPC trafficking from the peripheral blood to engrafted ST. Once grafts took, fluorescent (PKH26) dye–tagged HMVECs or EPCs were injected intravenously into mice engrafted with either normal or RA ST. ECs were allowed to circulate for at least 48 hours (for HMVECs) to 72 hours (for EPCs). The different incubation times for HMVECs and EPCs reflect the speed of incorporation of HMVECs compared to EPCs, as we found that mature HMVECs are recruited and integrated into the vasculature of engrafted synovium faster than EPCs.

Messenger RNA (mRNA) extraction and quantitative reverse transcription–polymerase chain reaction (PCR). SCID mouse grafts were snap-frozen and prepared for mRNA analysis. Total RNA was isolated from snap-frozen tissue using RNeasy Mini RNA isolation kits in conjunction with QIAshredders according to the protocol recommended by the manufacturer (Qiagen). Following isolation, RNA was quantified and checked for purity using a spectrophotometer (NanoDrop Technologies). Complementary DNA (cDNA) was then prepared using a Verso cDNA kit (Thermo Fisher Scientific). Quantitative PCR was performed using Platinum SYBR Green qPCR SuperMix-UDG according to the instructions of the manufacturer (Invitrogen). The primers used for human CXCL16 and GAPDH were the same as used previously (11). All samples were run in duplicate and analyzed using Eppendorf software.

Statistical analysis. Results are expressed as the mean ± SEM. Statistical significance was analyzed by Student's *t*-test. *P* values less than 0.05 were considered significant.

RESULTS

CXCR6 expression on ECs. Western blot analysis demonstrated that HMVECs expressed CXCR6 and that CXCR6 could be up-regulated by IL-1β

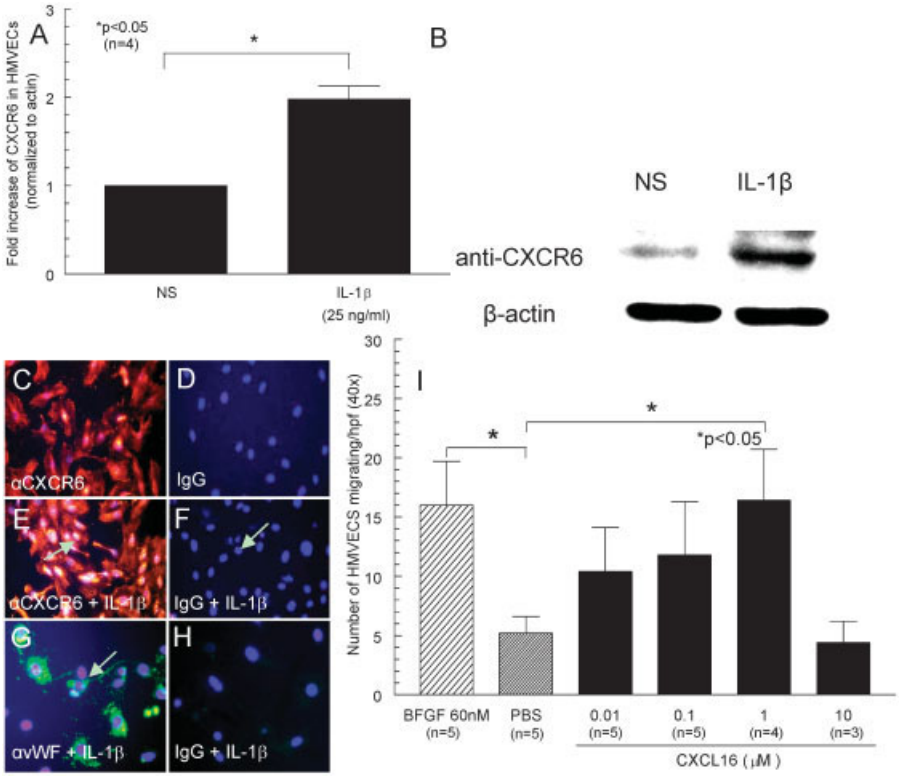

Figure 1. Human microvascular endothelial cells (HMVECs) express CXCR6 and are chemotactic for CXCL16. **A** and **B,** Western blots demonstrating expression of CXCR6 by HMVECs and up-regulation of this expression by interleukin-1β (IL-1β) (**B**), with the results normalized to β-actin and quantified (**A**). **C,** HMVEC expression of CXCR6 (red fluorescence staining). **D,** Control IgG staining of HMVECs. **E,** Intense CXCR6 staining in HMVECs (**arrow**) in response to stimulation with recombinant human IL-1β. **F,** Control IgG staining of HMVECs with IL-1β stimulation, showing a lack of staining for CXCR6 (**arrow**). **G,** Positive staining for von Willebrand factor (vWF) in HMVECs (**arrow**) in response to stimulation with IL-1β. **H,** Control IgG staining of HMVECs with IL-1β stimulation, showing induction of vWF. **I,** Dose-dependent migration of HMVECs toward CXCL16. HMVECs were chemotactic for CXCL16 at 1 μM, indicating that CXCL16 functions as an endothelial cell chemotactic factor. Values in **A** and **I** are the mean ± SEM; n represents the number of experiments. NS = no stimulus; bFGF = basic fibroblast growth factor; PBS = phosphate buffered saline. In **C–H,** original magnification × 40. Color figure can be viewed in the online issue, which is available at http://onlinelibrary.wiley.com/doi/10.1002/art.37981/abstract.

(Figures 1A and B). Anti-human CXCR6 was used as the primary antibody for detection of CXCR6 expression on HMVECs by immunofluorescence staining (Figure 1C). HMVECs expressed CXCR6, with further expression induced by IL-1β (Figures 1C and E). Control IgG staining is shown in Figures 1D, F, and H, and control staining for EC-specific vWF is shown in Figure 1G. CXCR6 was also expressed on EPCs (see below).

Induction of HMVEC chemotaxis by CXCL16. We tested the ability of CXCL16 to induce HMVEC migration in vitro. HMVEC chemotactic activity peaked with CXCL16 at a concentration of 1 μM and fell off at a higher concentration (Figure 1I).

Demonstration by in vitro capillary morphogenesis assay that CXCL16 is angiogenic in vitro. Capillary tube formation was determined by evaluation of nodular contacts between at least 3 endothelial cell tubes under blinded conditions, and the number of circular tube network formations was counted. Consistent with the chemotaxis results, CXCL16 induced tube formation (Figures 2A–C).

Evidence that HMVEC and EPC migration to engrafted tissue in ST SCID mouse chimeras is due to CXCL16. In both normal ST and RA ST mouse chimeras, there appeared to be a reduced number of scattered HMVECs migrating toward CXCL16 (Figures 2D and E). This can be explained by the finding of clumps of HMVECs apparently forming vasculature, thus having fewer scattered cells (Figure 2D). We also found that tumor necrosis factor α (TNFα), as well as CXCL16, up-regulated CXCL16 expression in vivo. SCID mouse grafts were snap-frozen and prepared for mRNA analy-

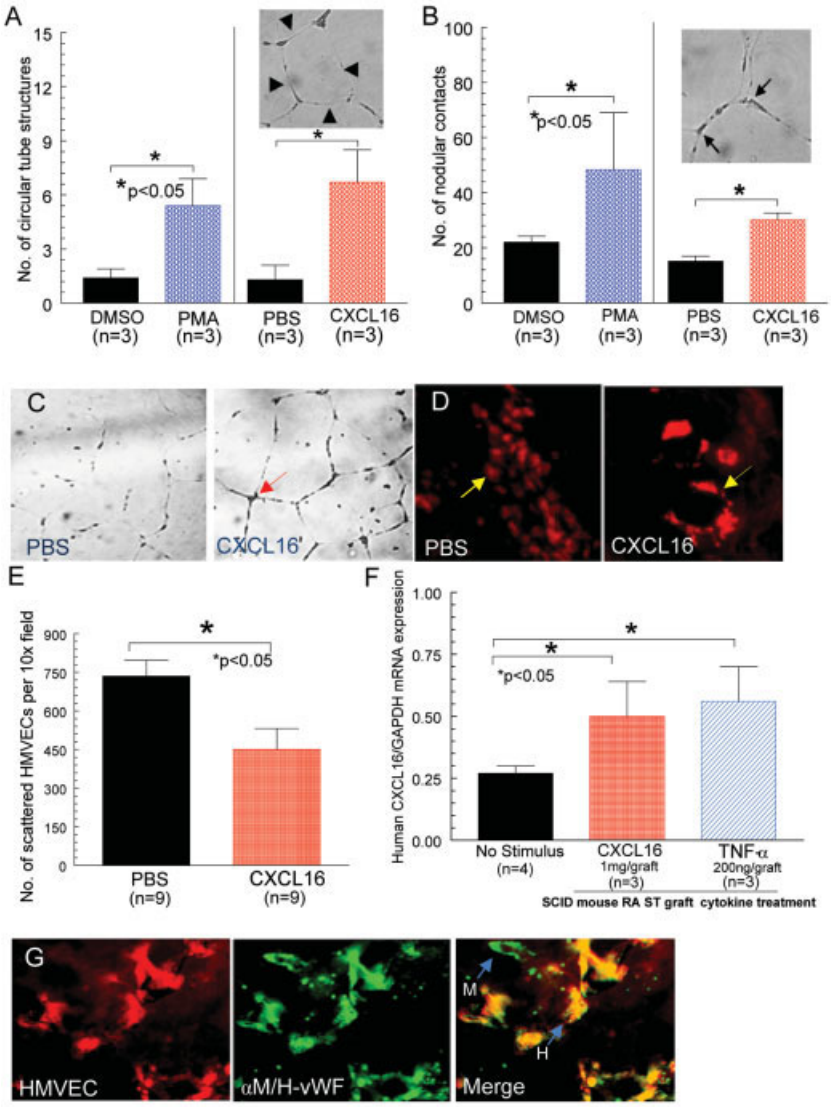

Figure 2. CXCL16 forms tubes in Matrigel and in human synovial tissue (ST) SCID mouse chimera. **A–C,** Examples of capillary tube formation, determined by evaluating circular tube networks (**A**) (**arrowheads**) and nodular contacts between endothelial cell tubes (**B** and **C**) (**arrows**). Tube formation was induced by treatment with CXCL16, compared to PBS. DMSO and 4-phorbol 12-myristate 13-acetate (PMA) were studied as negative and positive controls, respectively. Bars in **A** and **B** show quantification of the results, expressed as the mean ± SEM; n represents the number of experiments. **D,** Normal ST section, showing scattered dye-tagged HMVECs migrating in response to PBS (**arrow** in left panel) and clearly organized migration of dye-tagged HMVECs in response to intragraft administration of CXCL16 (**arrow** in right panel). **E,** Mean ± SEM numbers of scattered HMVECs observed in response to CXCL16 versus PBS in rheumatoid arthritis (RA) ST SCID mouse chimera; n represents the number of sections studied. Fewer scattered HMVECs were observed in response to CXCL16, likely due to HMVEC clumping. **F,** Mean ± SEM expression of CXCL16 mRNA in response to intragraft injection of CXCL16 or tumor necrosis factor α (TNFα), showing up-regulation of CXCL16 by both CXCL16 and TNFα; n represents the number of experiments. **G,** Serial section of PKH26 dye–tagged HMVECs migrating into engrafted human ST (left), serial section obtained from the same tissue sample and stained with fluorescein isothiocyanate–labeled rabbit anti-mouse/human (M/H) vWF (middle), and merged image of left and middle panels (right). Green color identifies mouse endothelium (**arrow M**) and yellow color identifies human endothelium (**arrow H**), demonstrating the formation of a true chimera. Experiments were performed in triplicate. In **A–D** and **G,** original magnification × 40. See Figure 1 for other definitions.

sis and, as seen in Figure 2F, both TNFα and CXCL16 up-regulated CXCL16 mRNA expression in the RA ST SCID mouse chimera system. Figure 2G shows HMVECs migrating into RA ST in the RA ST SCID mouse chimera, including images of red fluorescent HMVECs and of ST stained for both anti-mouse and

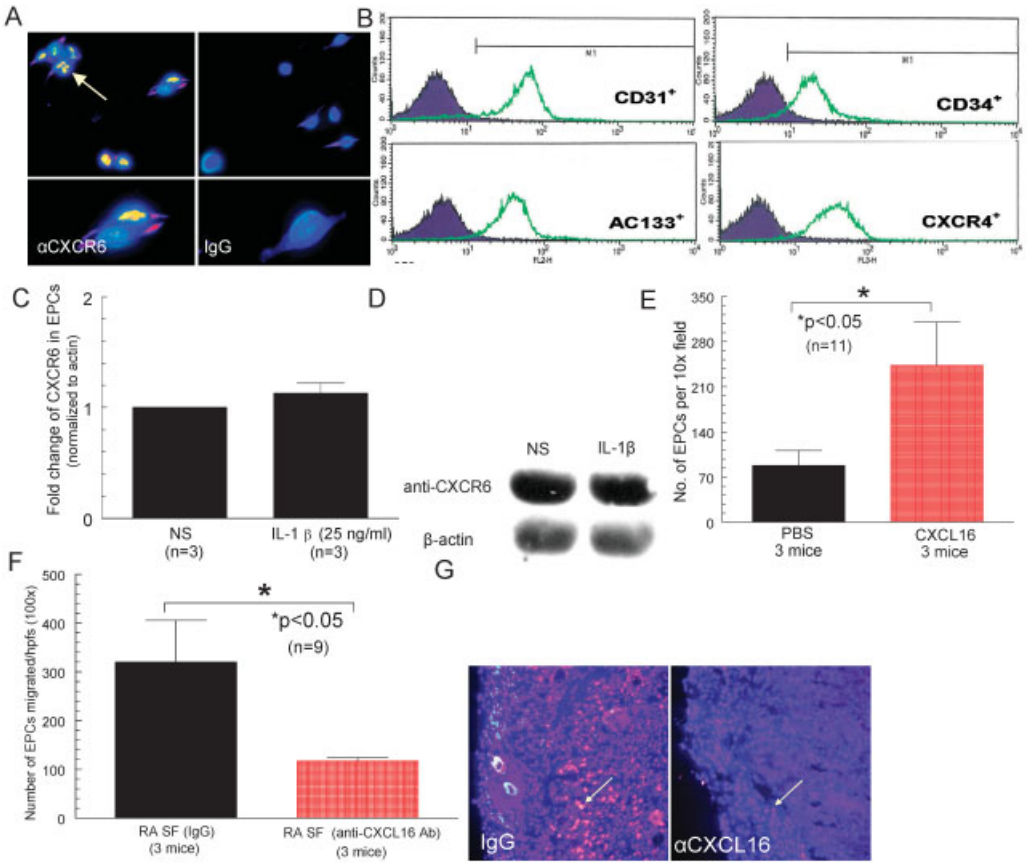

Figure 3. Endothelial progenitor cells (EPCs) express CXCR6 and migrate to CXCL16 in vivo. **A,** EPC expression of CXCR6 (yellow/orange fluorescence staining) (**arrow**). Control IgG staining is also shown. Original magnification × 40 in upper panels; × 400 in lower panels. **B,** Cell sorting and purification results. EPCs expressed CD31 and could also be identified and sorted by CD34 expression. More than 95% of these cells were AC133+. The isolated cell population also expressed CXCR4 (the receptor for stromal cell–derived factor 1α/CXCL12), even without any external stimuli (e.g., cytokines, lipopolysaccharide, 4-phorbol 12-myristate 13-acetate). **C** and **D,** Western blots demonstrating expression of CXCR6 by EPCs and no effect of IL-1β on this expression (**D**), with the results normalized to β-actin and quantified (**C**). Values are the mean ± SEM; n represents the number of experiments. **E** and **F,** Infiltration of EPCs into engrafted tissue in SCID mice engrafted with normal human synovium. EPC infiltration to engrafted tissue was increased ~3-fold in mice receiving intragraft injections of CXCL16 compared to mice receiving intragraft injections of PBS (**E**), and robust recruitment of fluorescent dye–tagged EPCs was observed in mice injected with sham-immunoneutralized rheumatoid arthritis (RA) synovial fluid (SF) compared to mice injected with CXCL16 antibody (Ab)–treated RA SF (**F**). Values are the mean ± SEM; n represents the number of sections counted. **G,** Images of fluorescence staining from the experiments described in **F,** demonstrating stronger recruitment of EPCs (**arrows**) in engrafted tissue injected with sham-immunoneutralized RA SF (left) than in engrafted tissue injected with CXCL16 antibody–treated RA SF (right). Original magnification × 10. See Figure 1 for other definitions. Color figure can be viewed in the online issue, which is available at http://onlinelibrary.wiley.com/doi/10.1002/art.37981/abstract.

anti-human vWF (stains all ECs), and a merged image revealing mouse and human endothelium integrated into the developing vasculature, indicating the formation of a true vascular chimera.

Human CD34+ EPCs can be isolated and characterized from cord blood. Anti-human CXCR6 was used as the primary antibody for detection of CXCR6 expression on human EPCs by immunofluorescence staining (Figure 3A). Central to all of these studies was our ability to generate pure populations of human EPCs. Cells were sorted and purified (Figure 3B), and we confirmed that pure populations of cells could be successfully isolated by receptor expression. We also showed, by Western blotting, that CXCR6 was highly expressed on EPCs but, unlike HMVECs, was not up-regulated by IL-1β (Figures 3C and D). EPCs also migrated toward the chemotactic stimulus (i.e., CXCL16), as evidenced by the observation that more fluorescent dye–tagged cells were found in the normal ST graft (Figure 3E), not appearing to form clumps

characteristic of HMVECs. Human cord blood preparations typically yield 1.5–2 $\times$ 10^6 CD133+ EPCs per preparation, with purities of >95%.

EPC migration to engrafted tissue injected with CXCL16-depleted RA SF. Injection of RA SF allows for neutralization studies, as a single chemokine can be neutralized from the RA SF before injection, for examination of its singular role in cellular recruitment and integration into the implanted tissue. Mice engrafted with normal ST that received intragraft injections of CXCL16-depleted RA SF (CXCL16- and sham-neutralized RA SF diluted 1:300 in PBS injected at 100 μl/graft) exhibited a robust reduction in EPC migration compared to the sham-depleted control group (n = 9 tissue sections from 3 different mice per group) (Figures 3F and G). This indicates that CXCL16 contained within the RA SF is directly responsible, in part, for EPC migration into normal human synovium.

Reduced joint swelling, histologic abnormality, and vascularity following K/BxN serum transfer in CXCR6$^{-/-}$ mice compared to WT mice. On day 9 after the initial injection of K/BxN serum, severe redness and swelling of the joints was observed in WT mice, but not in CXCR6$^{-/-}$ mice (Figure 4A). In addition, the articular index score and degree of joint swelling were significantly reduced in CXCR6$^{-/-}$ mice compared to WT mice beginning on day 5 (Figure 4B). Joint tissue sectioned from WT and CXCR6$^{-/-}$ mice with K/BxN serum–induced arthritis was stained with hematoxylin and eosin for histopathologic assessment. As shown in Figure 4C, cellular infiltration on day 9 was enhanced in WT mice compared to CXCR6$^{-/-}$ mice.

We also evaluated the number of vessels from the same tissue, based on vWF expression identified using immunofluorescence analysis. In these experiments, CXCR6-deficient mice with K/BxN serum–induced arthritis were shown to have a profound reduction in blood vessel numbers (Figures 4C and D). To validate these findings, we assessed concentrations of Hgb, a measure of total joint vascularity, in joint homogenates from the same animals, according to previously described methods (17,22). CXCR6$^{-/-}$ mice had significantly less Hgb (normalized to total protein) compared to arthritic WT mice (Figure 4D), confirming the histologic finding of reduced vascularity in the arthritic joints of CXCR6$^{-/-}$ mice.

Different CXCR6 regulation and CXCL16 signaling pathways in HMVECs and EPCs. Western blot experiments demonstrated that in HMVECs, CXCL16 up-regulated phospho-p38, phospho–ERK-1/2, and phospho-JNK, in a time-dependent manner

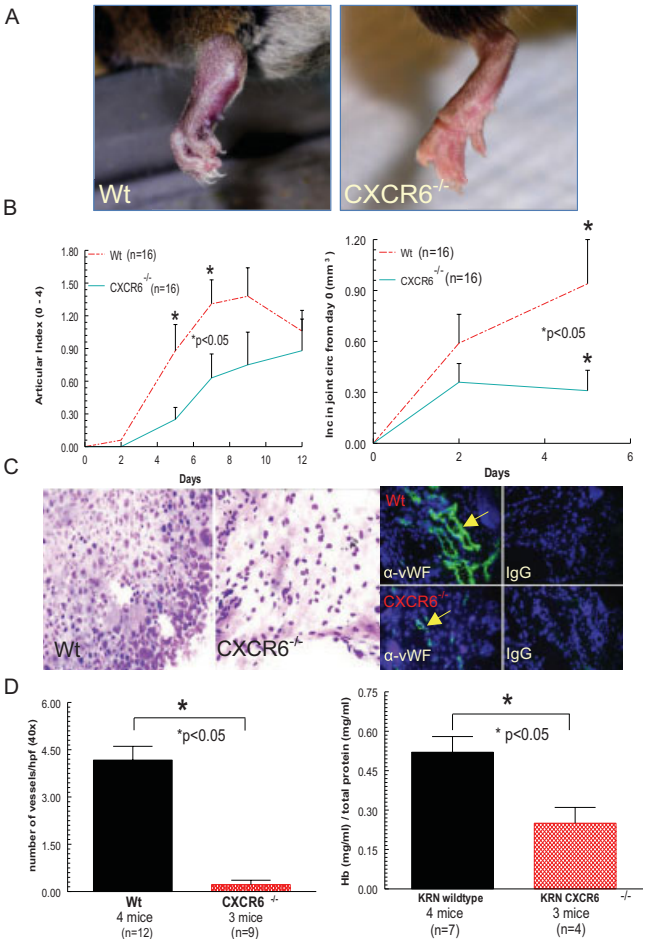

Figure 4. CXCR6 deficiency reduces joint inflammation and vascularity in K/BxN serum–induced arthritis. **A,** Representative clinical images of inflamed joints from mice with K/BxN serum–induced arthritis, showing significant edema and inflammation in the wild-type (WT) mouse but not the CXCR6$^{-/-}$ mouse. **B,** Articular index scores and increases in joint circumference (Inc in joint circ) in WT and CXCR6$^{-/-}$ mice (4 mice per group) following induction of arthritis via K/BxN serum transfer. Compared to WT mice, CXCR6$^{-/-}$ mice had significantly lower articular index scores on days 5 and 7 and significantly less joint swelling on day 5. Values are the mean ± SEM; n represents the number of joints assessed. **C,** Representative photomicrographs of 5-μm–thick sections obtained on day 9, showing increased cellular infiltration and severe tissue damage in the sample from a WT mouse compared to that from a CXCR6$^{-/-}$ mouse (left panels) (hematoxylin and eosin stained) and reduced vascularity (based on immunofluorescence staining for von Willebrand factor [vWF]) in the sample from the CXCR6$^{-/-}$ mouse (right panels); control IgG staining is also shown. Original magnification $\times$ 40. **D,** Number of blood vessels per high-power field (hpf) and concentration of hemoglobin (Hb) in joint homogenates from WT and CXCR6$^{-/-}$ mice on day 9. Both the number of vessels and the concentration of hemoglobin were significantly lower in the CXCR6$^{-/-}$ mice compared to the WT mice. Values are the mean ± SEM; n represents the number of sections counted. Color figure can be viewed in the online issue, which is available at http://onlinelibrary.wiley.com/doi/10.1002/art.37981/abstract.

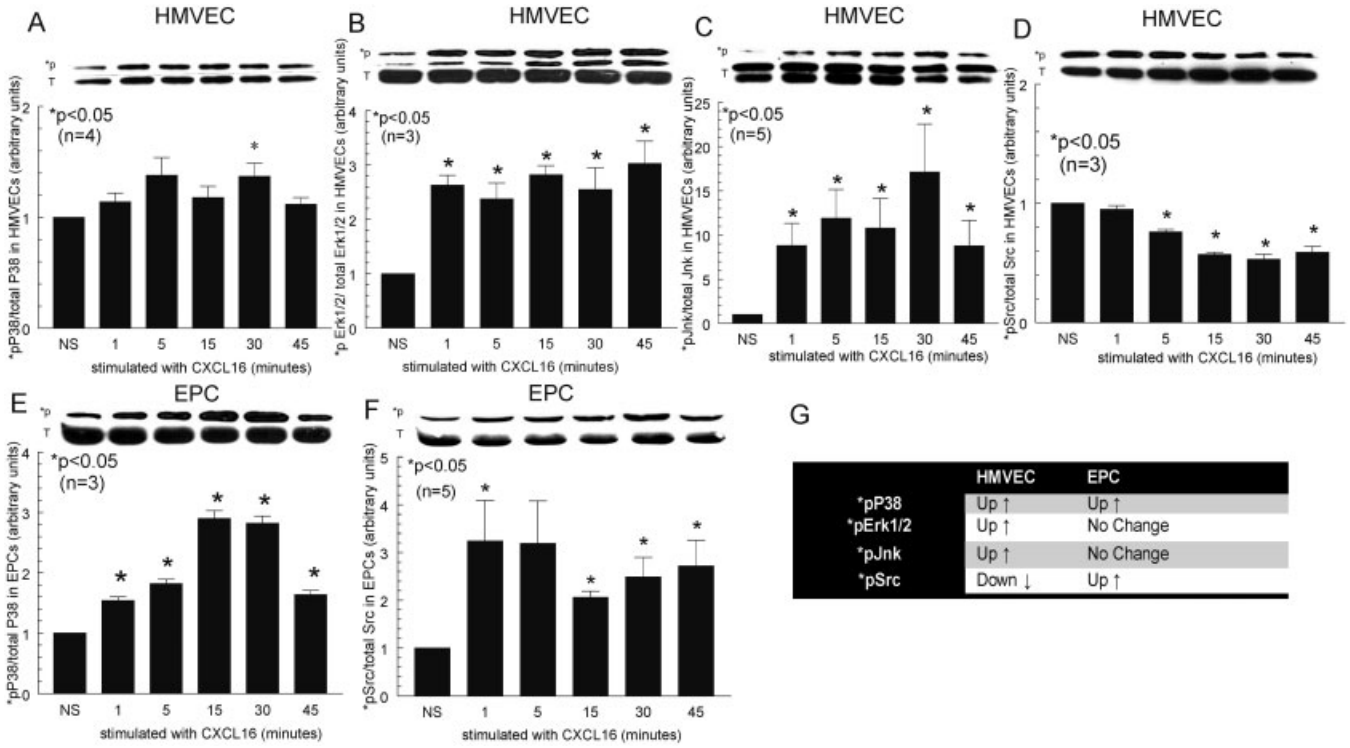

Figure 5. Signaling studies demonstrating activation of human microvascular endothelial cells (HMVECs) and endothelial progenitor cells (EPCs) by CXCL16. **A–F,** Representative blots from experiments assessing activation or down-regulation of p38 (**A**), ERK-1/2 (**B**), JNK (**C**), and Src (**D**) in HMVECs and of p38 (**E**) and Src (**F**) in EPCs. Upper and lower bands show the amount of each signaling molecule in phosphorylated form (p) and in total (phosphorylated and nonphosphorylated) (T), respectively; therefore, for each signaling molecule the upper blot is an indication of the amount of phosphorylated protein contained in the lower band. Results were quantified, and bars show the mean ± SEM. *P* values are versus no stimulus (NS). In HMVECs, phospho-p38, phospho-ERK-1/2, and phospho-JNK were activated in response to CXCL16, whereas phospho-Src was down-regulated. In EPCs, phospho-p38 and phospho-Src were activated in response to CXCL16. **G,** Summary of the signaling results in HMVECs and EPCs in response to CXCL16. Of note is the finding that both cell types signaled through phospho-p38, indicating that the angiogenic and/or vasculogenic activity of CXCL16 could be targeted by phospho-p38 inhibition.

(Figures 5A–C), whereas phospho-Src was down-regulated by CXCL16 (Figure 5D). In contrast, EPCs were shown to signal through phospho-Src in response to CXCL16, with up-regulation of phospho-p38 demonstrated as well (Figures 5E and F). Thus, only phospho-p38 was similarly regulated in HMVECs and EPCs, with the other pathways differing between the two cell types (Figure 5G).

Reduced leukocyte recruitment following K/BxN serum transfer in CXCR6$^{-/-}$ mice compared to WT mice. In the joints of WT mice with K/BxN serum–induced arthritis, prominent CD3 and CD14 expression was observed (Figure 6A). In contrast, in CXCR6-deficient mice with K/BxN serum–induced arthritis, the numbers of both CD3+ cells and CD14+ cells were profoundly reduced (Figures 6B and C).

DISCUSSION

RA is a debilitating inflammatory joint disease in which microvascular expansion in the joint lining (synovium) is a characteristic finding. Synovial neovascularization occurs presymptomatically and is critical for disease progression (23). Studies in rodents have shown that inhibition of angiogenesis results in suppression of arthritis as well (24); however, there are limited data to quantify the effectiveness of therapies targeting potent angiogenic chemokines or chemokine receptors. Notably, Jodon de Villeroche and colleagues (25) have shown that increased numbers of circulating EPCs in patients with RA correlate with the 28-joint Disease Activity Score (26), signifying that EPCs are likely elevated and recruited to inflamed tissue for the purposes of synovial

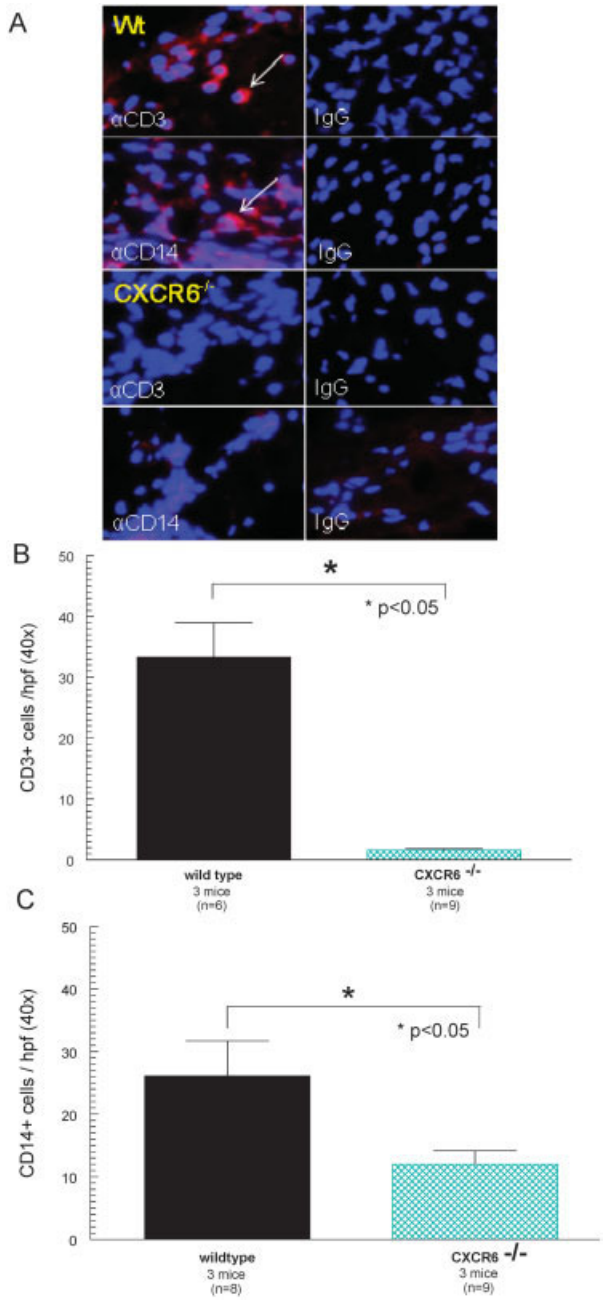

Figure 6. CXCR6 deficiency results in reduced leukocyte recruitment to inflamed joint tissue. Joints from wild-type (WT) and CXCR6$^{-/-}$ mice were harvested on day 9 of K/BxN serum–induced arthritis and CD3 and CD14 expression was assessed by immunofluorescence staining. **A,** Prominent expression of CD3 and CD14 (**arrows**) in the cells of WT mice, which was profoundly reduced in CXCR6$^{-/-}$ mice. Control IgG staining is also shown. Original magnification × 40. **B** and **C,** Quantification of the number of CD3+ cells (**B**) and CD14+ cells (**C**) per high-power field (hpf), showing significant reductions of both CD3 and CD14 in the joints of CXCR6$^{-/-}$ mice. Values are the mean ± SEM; n represents the fields counted per section. Color figure can be viewed in the online issue, which is available at http://onlinelibrary.wiley.com/doi/10.1002/art.37981/abstract.

vasculogenesis. Previous studies have demonstrated reduced severity of arthritis in mice that lack CXCL16 (27), suggesting that CXCR6 and its ligand CXCL16 may be important mediators of arthritis development. Based on the expression of CXCR6 on HMVECs and EPCs and the highly elevated expression of CXCL16 in RA SF (11), we believe CXCL16 is central to this process.

Using a combined in vitro and in vivo approach, we examined possible environmental cues that might direct the migration, differentiation, and functional incorporation of HMVECs and EPCs into the microcirculatory system. Initially, we immunostained HMVECs and EPCs to validate their expression of CXCR6, and confirmed that CXCR6 expression by HMVECs could be up-regulated in response to a proinflammatory stimulus. Next, we examined the ability of CXCL16 to recruit HMVECs and form tubes in vitro. Using a modified Boyden chemotaxis system, we found that HMVECs migrate to CXCL16 in a dose-dependent manner. We then showed that HMVECs respond to CXCL16 in Matrigel by forming tubes, in accordance with our chemotaxis findings.

To examine the behavior of HMVECs in response to CXCL16 in vivo, we injected CXCL16 intragraft into normal ST SCID mouse chimeras and found that well-integrated HMVECs could be observed in the engrafted synovium 48 hours postinjection, not as scattered cells but as clumps of cells that appear to be forming vessels and chimeric nodes with the surrounding murine vasculature. EPCs also migrated in the SCID mouse chimera system, and we showed that by depleting RA SF of CXCL16, we could suppress EPC recruitment by approximately two-thirds, confirming that CXCL16 contained within RA SF induces EPC migration from the peripheral blood directly into engrafted human ST. We also defined the CXCL16 signaling pathways for both types of ECs and observed interesting divergences between HMVECs (the mature phenotype) and EPCs. We found that phospho-p38 expression was up-regulated in both HMVECs and EPCs in response to CXCL16, whereas phospho-Src expression was up-regulated in EPCs but down-regulated in HMVECs. In addition, HMVECs signaled in response to CXCL16 via phospho-ERK-1/2 and phospho-JNK, whereas EPCs did not. We surmise that ECs may signal differently in response to CXCL16 based primarily upon the maturity of the cell.

Although we demonstrated that HMVECs and EPCs readily migrated in the SCID mouse chimera, HMVECs integrated into the established vasculature at

a much faster pace compared to EPCs, reminiscent of an angiogenic response. Conversely, EPCs appeared to home much like mononuclear cells (11) and did not incorporate into existing vasculature as quickly, resembling a more vasculogenic response. These findings suggest that CXCL16 is a robust agonist of both angiogenesis (HMVEC migration and incorporation) and vasculogenesis (EPC migration), promoting both de novo blood vessel formation in RA synovium and expansion of the existing capillary network, by two independent mechanisms. We showed that both CXCL16 and TNFα up-regulated CXCL16 mRNA expression in the SCID mouse chimera, defining an amplification step for the expression of CXCL16 in vivo. Based on these findings, it is tempting to speculate that by inhibiting EC CXCL16 signaling via phospho-p38, both the angiogenic and the vasculogenic processes stimulated by CXCL16 could be disrupted, perhaps identifying a legitimate target for inhibition of CXCL16-induced EC activity within the RA joint.

We further validated our findings in experiments in which K/BxN serum was injected into CXCR6$^{-/-}$ mice. These studies showed that arthritis development is attenuated in mice lacking CXCR6 compared to WT mice. Indeed, while WT mice clearly displayed a robust inflammatory phenotype, including functional deficits, following arthritis induction, their CXCR6$^{-/-}$ counterparts were comparatively only mildly affected, suggesting that CXCR6 is a critical mediator of arthritis development. This was supported by histologic findings showing reduced inflammation in the joint tissue of CXCR6$^{-/-}$ mice after K/BxN serum transfer. We also demonstrated reduced Hgb content in joint homogenates from K/BxN serum–treated CXCR6$^{-/-}$ mice, as well as profound reductions in the number of cells expressing vWF (EC marker), CD3 (T cell marker), and CD14 (macrophage marker) in the joint tissue of these mice compared to similarly-treated age- and weight-matched WT mice.

It should be noted that CXCL16 can recruit other cells, apart from ECs, that may produce angiogenic factors, such as vascular endothelial cell growth factor (VEGF). Indeed, our data demonstrate that CXCR6 deficiency results in profound reductions in monocytes known to produce VEGF. However, our results, including HMVEC chemotaxis and tube formation in Matrigel (both performed in the absence of other cell types), provide strong evidence that CXCL16 has a direct role in the stimulation of angiogenic activity. Although HMVECs are also capable of producing VEGF, which may potentially confound our findings, it is important to point out that our control experiments using only PBS did not show substantial angiogenic activity in either the HMVEC migration or tube formation assays. We then confirmed these findings in vivo using both HMVECs and EPCs (both shown to express CXCR6, the only known CXCL16 receptor). These results, when considered in total, lead us to the conclusion that CXCL16 functions as both an angiogenic mediator and a potent leukocyte recruitment factor.

Based on our findings demonstrating that CXCL16 is involved in blood vessel formation in arthritic joints, it is possible that the CXCL16/CXCR6 pathway may be a primary pathway in the recruitment of EPCs from the bone marrow. This is supported by a previous report that very high percentages of mesenchymal stem cells from both humans and mice ($>$90%) express CXCR6 (10). Consistent with this, we have shown that EPCs and HMVECs prominently express CXCR6, which might explain the significant reductions in vascularity in CXCR6$^{-/-}$ mice during arthritis development. Interestingly, we also discovered that HMVECs and EPCs regulate the expression of CXCR6 differently when stimulated with IL-1β, with rapid up-regulation of HMVECs, but not EPCs, in response to IL-1β. Notably, we found that EPCs robustly express CXCR6 without a need for further stimulation. It is tempting to speculate that EPCs may require this receptor to navigate from the bone marrow to inflamed tissue such as the RA joint.

It has been argued that EPCs may not be a viable target for RA therapy, as these cells have not been observed in appreciable numbers in inflamed synovium. However, this same observation also raised concerns as to whether EPC populations are truly being monitored in vivo, and has imposed tremendous limitations on the assessment of the biologic function of EPCs as well as their potential use as a therapeutic target (28). In support of the notion that EPCs have a proinflammatory role, it was previously demonstrated that human EPCs readily migrate to RA ST, compared to normal ST, in the SCID mouse chimera (13), and these findings are in complete accordance with the present results obtained using a similar chimera model system. The most significant finding in the present study is that EPCs migrate toward RA SF in vivo and that this effect can be abrogated with the removal of CXCL16. We also have shown that EC signaling pathways in response to CXCL16 are different depending upon the maturity of ECs and have demonstrated where the different pathways intersect, possibly identifying suitable targets for intervention strategies. Overall, the present results provide further evidence that CXCL16 is a central proinflammatory chemokine in joints affected by RA, promoting both vasculogenesis and angiogenesis and

contributing to the expansion of the neovasculature in rheumatoid synovium.

AUTHOR CONTRIBUTIONS

All authors were involved in drafting the article or revising it critically for important intellectual content, and all authors approved the final version to be published. Drs. Isozaki and Ruth had full access to all of the data in the study and take responsibility for the integrity of the data and the accuracy of the data analysis.

Study conception and design. Isozaki, Amin, Arendt, Ruth.

Acquisition of data. Isozaki, Arbab, Haas, Amin, Arendt, Ruth.

Analysis and interpretation of data. Isozaki, Amin, Arendt, Koch, Ruth.

REFERENCES

1. Firestein GS. Evolving concepts of rheumatoid arthritis. Nature 2003;423:356–61.
2. Corrigall VM, Panayi GS. Autoantigens and immune pathways in rheumatoid arthritis. Crit Rev Immunol 2002;22:281–93.
3. Paleolog EM. Angiogenesis in rheumatoid arthritis. Arthritis Res 2002;4 Suppl 3:S81–90.
4. Folkman J, Haudenschild C. Angiogenesis by capillary endothelial cells in culture. Trans Ophthalmol Soc U K 1980;100:346–53.
5. Masuda H, Asahara T. Post-natal endothelial progenitor cells for neovascularization in tissue regeneration. Cardiovasc Res 2003;58: 390–8.
6. Haas CS, Amin MA, Ruth JH, Allen BL, Ahmed S, Pakozdi A, et al. In vivo inhibition of angiogenesis by interleukin-13 gene therapy in a rat model of rheumatoid arthritis. Arthritis Rheum 2007;56:2535–48.
7. Volin MV, Woods JM, Amin MA, Connors MA, Harlow LA, Koch AE. Fractalkine: a novel angiogenic chemokine in rheumatoid arthritis. Am J Pathol 2001;159:1521–30.
8. Koch AE, Polverini PJ, Kunkel SL, Harlow LA, DiPietro LA, Elner VM, et al. Interleukin-8 as a macrophage-derived mediator of angiogenesis. Science 1992;258:1798–801.
9. Szekanecz Z, Koch AE. Chemokines and angiogenesis. Curr Opin Rheumatol 2001;13:202–8.
10. Chamberlain G, Wright K, Rot A, Ashton B, Middleton J. Murine mesenchymal stem cells exhibit a restricted repertoire of functional chemokine receptors: comparison with human. PLoS One 2008;3:e2934.
11. Ruth JH, Haas CS, Park CC, Amin MA, Martinez RJ, Haines GK III, et al. CXCL16-mediated cell recruitment to rheumatoid arthritis synovial tissue and murine lymph nodes is dependent upon the MAPK pathway. Arthritis Rheum 2006;54:765–78.
12. Distler JH, Beyer C, Schett G, Luscher TF, Gay S, Distler O. Endothelial progenitor cells: novel players in the pathogenesis of rheumatic diseases [review]. Arthritis Rheum 2009;60:3168–79.
13. Silverman MD, Haas CS, Rad AM, Arbab AS, Koch AE. The role of vascular cell adhesion molecule 1/very late activation antigen 4 in endothelial progenitor cell recruitment to rheumatoid arthritis synovium. Arthritis Rheum 2007;56:1817–26.
14. Moore XL, Lu J, Sun L, Zhu CJ, Tan P, Wong MC. Endothelial progenitor cells' "homing" specificity to brain tumors. Gene Ther 2004;11:811–8.
15. Katschke KJ Jr, Rottman JB, Ruth JH, Qin S, Wu L, LaRosa G, et al. Differential expression of chemokine receptors on peripheral blood, synovial fluid, and synovial tissue monocytes/macrophages in rheumatoid arthritis. Arthritis Rheum 2001;44:1022–32.
16. Ruth JH, Rottman JB, Katschke KJ Jr, Qin S, Wu L, LaRosa G, et al. Selective lymphocyte chemokine receptor expression in the rheumatoid joint. Arthritis Rheum 2001;44:2750–60.
17. Park CC, Morel JC, Amin MA, Connors MA, Harlow LA, Koch AE. Evidence of IL-18 as a novel angiogenic mediator. J Immunol 2001;167:1644–53.
18. Kumar P, Hosaka S, Koch AE. Soluble E-selectin induces monocyte chemotaxis through Src family tyrosine kinases. J Biol Chem 2001;276:21039–45.
19. Ruth JH, Volin MV, Haines GK III, Woodruff DC, Katschke KJ Jr, Woods JM, et al. Fractalkine, a novel chemokine in rheumatoid arthritis and in rat adjuvant-induced arthritis. Arthritis Rheum 2001;44:1568–81.
20. Monach P, Hattori K, Huang H, Hyatt E, Morse J, Nguyen L, et al. The K/BxN mouse model of inflammatory arthritis: theory and practice. Methods Mol Med 2007;136:269–82.
21. Woods JM, Katschke KJ, Volin MV, Ruth JH, Woodruff DC, Amin MA, et al. IL-4 adenoviral gene therapy reduces inflammation, proinflammatory cytokines, vascularization, and bony destruction in rat adjuvant-induced arthritis. J Immunol 2001;166: 1214–22.
22. Ruth JH, Amin MA, Woods JM, He X, Samuel S, Yi N, et al. Accelerated development of arthritis in mice lacking endothelial selectins. Arthritis Res Ther 2005;7:R959–70.
23. Koch AE. Angiogenesis as a target in rheumatoid arthritis. Ann Rheum Dis 2003;62 Suppl 2:ii60–7.
24. Peacock DJ, Banquerigo ML, Brahn E. Angiogenesis inhibition suppresses collagen arthritis. J Exp Med 1992;175:1135–8.
25. Jodon de Villeroche V, Avouac J, Ponceau A, Ruiz B, Kahan A, Boileau C, et al. Enhanced late-outgrowth circulating endothelial progenitor cell levels in rheumatoid arthritis and correlation with disease activity. Arthritis Res Ther 2010;12:R27.
26. Prevoo ML, van 't Hof MA, Kuper HH, van Leeuwen MA, van de Putte LB, van Riel PL. Modified disease activity scores that include twenty-eight–joint counts: development and validation in a prospective longitudinal study of patients with rheumatoid arthritis. Arthritis Rheum 1995;38:44–8.
27. Nanki T, Shimaoka T, Hayashida K, Taniguchi K, Yonehara S, Miyasaka N. Pathogenic role of the CXCL16–CXCR6 pathway in rheumatoid arthritis. Arthritis Rheum 2005;52:3004–14.
28. Mellick AS, Plummer PN, Nolan DJ, Gao D, Bambino K, Hahn M, et al. Using the transcription factor inhibitor of DNA binding 1 to selectively target endothelial progenitor cells offers novel strategies to inhibit tumor angiogenesis and growth. Cancer Res 2010;70:7273–82.